Dynamic trafficking and delivery of connexons to the plasma membrane and accretion to gap junctions in living cells

Undine Lauf*, Ben N. G. Giepmans*†, Patricia Lopez*, Sébastien Braconnot*, Shu-Chih Chen‡, and Matthias M. Falk*§

*Department of Cell Biology, The Scripps Research Institute, 10550 North Torrey Pines Road, La Jolla, CA 92037; †Division of Cellular Biochemistry, The Netherlands Cancer Institute, Plesmanlaan 121, 1066 CX, Amsterdam, The Netherlands; and ‡Molecular Medicine, Northwest Hospital, 21720 23rd Drive Southeast, Suite 101, Bothell, WA 98021

Edited by Marilyn Gist Farquhar, University of California at San Diego, La Jolla, CA, and approved June 7, 2002 (received for review January 30, 2002)

Certain membrane channels including acetylcholine receptors, gap junction (GJ) channels, and aquaporins arrange into large clusters in the plasma membrane (PM). However, how these channels are recruited to the clusters is unknown. To address this question, we have investigated delivery of GJ channel subunits (connexons) assembled from green fluorescent protein (GFP)-tagged connexin 43 (Cx43) to the PM and GJs in living cells. Fluorescence-photobleaching of distinct areas of Cx43-GFP GJs demonstrated that newly synthesized channels were accrued to the outer margins of channel clusters. Time-lapse microscopy further revealed that connexons were delivered in vesicular carriers traveling along microtubules from the Golgi to the PM. Routing and insertion of connexons occurred predominantly into the nonjunctional PM. These PM connexons can move laterally as shown by photobleaching and thus, can reach the margins of channel clusters. There, the apposing PMs are close enough to allow connexons to dock into complete GJ channels. When connexon delivery to the PM was inhibited by brefeldin A, or nocodazole pretreatment, the PM pool initially enabled connexon accrual to the clusters but further accrual was inhibited upon depletion. Taken together, our results indicate that GJ channel clusters grow by accretion at their outer margins from connexon subunits that were delivered to the nonjunctional PM, and explain how connexons in the PM can function in intra-/extracellular signaling before GJ channel formation and direct cell–cell communication.

Cx43 | GFP | photo-bleaching | secretion | time-lapse microscopy

A number of membrane proteins, including acetylcholine receptors, certain aquaporins, tight junction subunits, and gap junction (GJ) channels arrange into densely packed clusters, arrays, or strands in the plasma membrane (PM). GJ channels, in particular, have been known for many years to arrange extensively into tightly packed two-dimensional arrays, termed GJ plaques, that can consist of thousands of channels and extend to several micrometers in diameter (1–3). However, how these multiunit structures are assembled and new channels are added to the cluster has remained largely elusive. To address this fundamental question, we have investigated in living cells how newly synthesized GJ channels are recruited to the PM and GJs.

GJ channels are double membrane protein structures that mediate direct cell–cell communication by allowing the passage of molecules up to ≈1 kDa from one cell to the other (4). Channels form by head-to-head docking of two connexons (hemi-channels), each provided by one of two neighboring cells, thereby creating hydrophilic pores across the membranes (5). Connexons are composed of six polytopic transmembrane protein subunits, termed connexins (Cx). Cxs comprise a large gene family predicted to consist of 20 isoforms in humans alone (6), allowing the synthesis of a large number of different connexons and GJ channels.

The investigations of others and our previous work have shown that Cxs are cotranslationally integrated into the endoplasmic reticulum membrane (7) followed by their assembly into hexameric connexons (8, 9). Subcellular fractionation studies (7, 10) and immuno-colocalization analyses (10–12) indicated that Cxs pass through the Golgi apparatus to reach the PM (reviewed in ref. 13).

At least three possibilities are conceivable by which newly synthesized connexons are recruited to GJs. (*i*) Connexon-containing transport vesicles may fuse with the PM within the plaques (Fig. 1*A*); (*ii*) transport vesicles fuse with the PM at the outer margin of plaques (Fig. 1*B*); and/or (*iii*) transport vesicles fuse with nonjunctional PMs and connexons drift in the PMs to the plaques where they can dock into complete GJ channels (Fig. 1*C*).

To investigate how newly synthesized GJ channels are recruited to the channel clusters, the C terminus of the most widely distributed connexin (Cx43) was tagged with green fluorescent protein (GFP), or its cyan color variant (CFP), and tagged Cxs were expressed in living cells. Previously, we and others have shown that C-terminal GFP-tagged Cxs traffic and assemble into functional GJ channels indistinguishable from wild-type Cxs (12, 14, 15). Although trafficking and clustering of connexons has been investigated in living cells (14, 15), none of these studies were aimed at discovering how GJ channel clusters grow, and where the newly recruited channels were delivered.

We have permanently photo-bleached the GFP-fluorescence of selected areas of Cx43-GFP GJ plaques, and monitored delivery of newly synthesized channels to the plaques over time. In addition, to investigate where the newly recruited channels originated, we have imaged Cx43-GFP, or Cx43-CFP secretion, and PM delivery by time-lapse microscopy. Finally, dynamics of PM connexons was investigated by fluorescence recovery after photo-bleaching (FRAP) and fluorescence loss in photo-bleaching (FLIP) experiments. Results suggest that connexons are transported from the Golgi to the PM via vesicular transport along microtubules (MTs). Connexon-containing constitutive transport vesicles then fuse and deliver connexons all over the nonjunctional PM. PM connexons can move laterally to reach GJs where they register, dock, and fuse at the outer plaque margins.

Materials and Methods

cDNA Constructs. Construction of fluorescent protein-tagged Cx43 has been described (12). YFP-α-tubulin was derived from pEYFP-Tub (CLONTECH).

Cell Lines, Cell Culture, and Transfection Conditions. Human epitheloid cervix carcinoma (HeLa) and T51B rat liver epithelial cells

This paper was submitted directly (Track II) to the PNAS office.

Abbreviations: BFA, brefeldin A; CFP, cyan fluorescent protein; Cx, connexin; FLIP, fluorescence loss in photo-bleaching; FRAP, fluorescence recovery after photo-bleaching; GFP, green fluorescent protein; GJ, gap junction; MT, microtubule; PM, plasma membrane.

§To whom reprint requests should be addressed. E-mail: mfalk@scripps.edu.

www.pnas.org/cgi/doi/10.1073/pnas.162055899

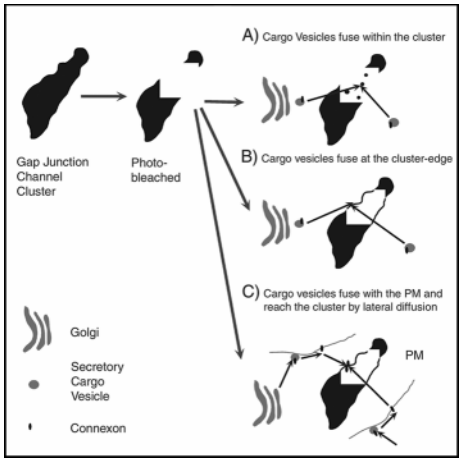

Fig. 1. Schematic representation of possible mechanisms by which clusters of GJ channels can be assembled (*A–C*), and of the FRAP method that was used to investigate this process in living cells.

were used in this study. Both cell lines were maintained under standard conditions as described (12). Cells (60–70% confluency) were transfected with Superfect Transfection Reagent (Qiagen, Valencia, CA) following manufacturer's instructions. For simultaneous labeling of Cx43 and MTs, respective cDNAs were mixed before transfection. A stable HeLa-22 cell line allowing regulation of Cx43-GFP expression was used in this study as well (described in *Supporting Text*, which is published as supporting information on the PNAS web site, www.pnas.org).

Organelle Staining, and Disruption of Subcellular Structures. Golgi membranes were stained in living cells with BODIPY TR ceramide (Molecular Probes) according to the manufacturer's instructions at least 30 min before photo-bleaching of GJs. To disrupt the Golgi complex, cells were placed in medium containing 5 μg/ml brefeldin A (BFA) (diluted from a 5 mg/ml stock solution in ethanol) for at least 30 min before photo-bleaching. MTs were labeled by transfecting cells with pEYFP-Tub, and depolymerized by placing cells in medium containing 100 μg/ml nocodazole (diluted from a 100 mg/ml stock solution in DMSO) for at least 30 min before photo-bleaching.

Microscopy and Image Processing. *Wide-field fluorescence deconvolution microscopy and time-lapse imaging.* High-resolution time-lapse images were acquired using a DeltaVision Model 283 (Applied Precision, Issaquah, WA) microscope as described (12). To resolve the rapid trafficking of post-Golgi carriers, image sequences were acquired at up to two images per second. Image sequences were analyzed using SOFTWORX (Applied Precision), NIH IMAGE (National Institutes of Health, Bethesda), and PHOTOSHOP (Adobe Systems, San Jose, CA) software.

Laser scanning confocal microscopy and photo-bleaching. Cx43-GFP fluorescence of GJ plaques and PMs was photo-bleached using a Bio-Rad MRC1024 confocal microscope system in combination with Zeiss 100× (Plan-Neofluar, NA 1.30) or 63× (Plan-Apochromat, NA 1.40) oil immersion lenses. Transfected HeLa cells grown on cover glasses (12) were mounted next day in a live-cell chamber (Focht FCS2, Bioptechs, Butler, PA) kept at 37°C either without further treatment, or after incubating cells in BFA or nocodazole. To determine qualitative FRAP of GJ plaques, cells were imaged at low magnification (zoom level 1–3, 512 × 512 pixels) and laser power of 1–3% (= prebleach image). Next, the laser was zoomed (level 10–20), power increased to 100%, and the area scanned 3–8 times until fluorescence was removed through the entire depth of the cell. The laser was zoomed out again and its power reduced to original settings. Reappearance of fluorescence was recorded by imaging the plaque repeatedly for up to 2 h (= postbleach images). At each time point optical sections were collected in 0.2-μm steps covering the thickness of the plaques (3–5 μm), and volume reconstructions were rendered using Bio-Rad LASERSHARP software. Numbers of plaques in untreated cells were compared with BFA- and nocodazole-treated cells (n = 55) for significant differences by using the Fischer exact test of INSTAT software (GraphPad, San Diego).

To determine qualitative FRAP of PM connexons, square areas 18 × 18 μm (n = 12) and 9 × 9 μm (n = 3) in size were photo-bleached through the entire depth of the cells, and recovery of fluorescence was imaged every 20 s until the intensity had reached a steady plateau. Postbleach imaging did not result in a significant loss of fluorescence over time (Fig. 5*A*) and was neglected. Residual fluorescence intensity was determined by measuring the intensity of a small central region of the bleached square area in the first postbleach images (n = 15). To calculate mobile and immobile fractions, fluorescence of selected square areas was photo-bleached to remove fluorescence of immobile, or slowly moving bright fluorescent intracellular spots, and after complete recovery ($t \geq 7$ min) was bleached again before recovery images were taken (Fig. 5*B*). Recovery measurements (n = 3) were quantified by fitting normalized fluorescence intensities of bleached areas to a sigmoidal least squares curve by using the nonlinear regression algorithm of PRISM software (GraphPad). FLIP experiments were done by bleaching a square area (18 × 18 μm) at 0, 2, 4, 7, 10, 15, and 20 min, and decrease of fluorescence intensity in the unbleached region of the cells was determined.

Results

GJ Channel Clusters Grow by Accretion of Newly Synthesized Channels to the Outer Cluster Margins. To investigate how GJ channels are added to GJ channel clusters, we photo-bleached the GFP-fluorescence of selected areas of Cx43-GFP GJs that were assembled in transfected HeLa cells and were either visible on their plane surface or on their side (boxed area shown in the prebleach images of Fig. 2). Then, entire junctions were observed and imaged repeatedly over time and volume views covering the entire thickness of the plaques were reconstructed (postbleach images of Fig. 2).

In all instances, new fluorescence reappeared simultaneously along both sides of the plaques within 10–20 min after bleaching. Fluorescence reappeared homogeneously throughout the entire length of the bleached areas as a homogenous fine line that steadily increased in width (post bleach images of Fig. 2*A*). Similar results were obtained when plaques viewed on their side were photo-bleached (Fig. 2*B*).

In total we have bleached and recorded 55 plaques. Thirty-two plaques were recorded from cells without drug pretreatment. Nineteen plaques were recorded after treating the cells with BFA, and four plaques were recorded after treating the cells with nocodazole. Results of all experiments are summarized in Table 1.

Blocking Connexon Secretion Allowed Initial Recovery but Inhibited Further Channel Accrual. To investigate whether accrual of channels to the cluster edge depended on delivery of connexons to the PM, we inhibited secretion of newly synthesized connexons by treating the cells with BFA 30 min before photo-bleaching. Golgi membranes were labeled in living cells and Golgi disruption after BFA-treatment was verified by the redistribution of the label (Fig. 2*C*, first two panels). Only GJ plaques between cells in which both Golgi structures were disrupted were bleached.

GJs that were bleached in BFA-treated cells showed initial appearance of new fluorescence along the edge of the plaques

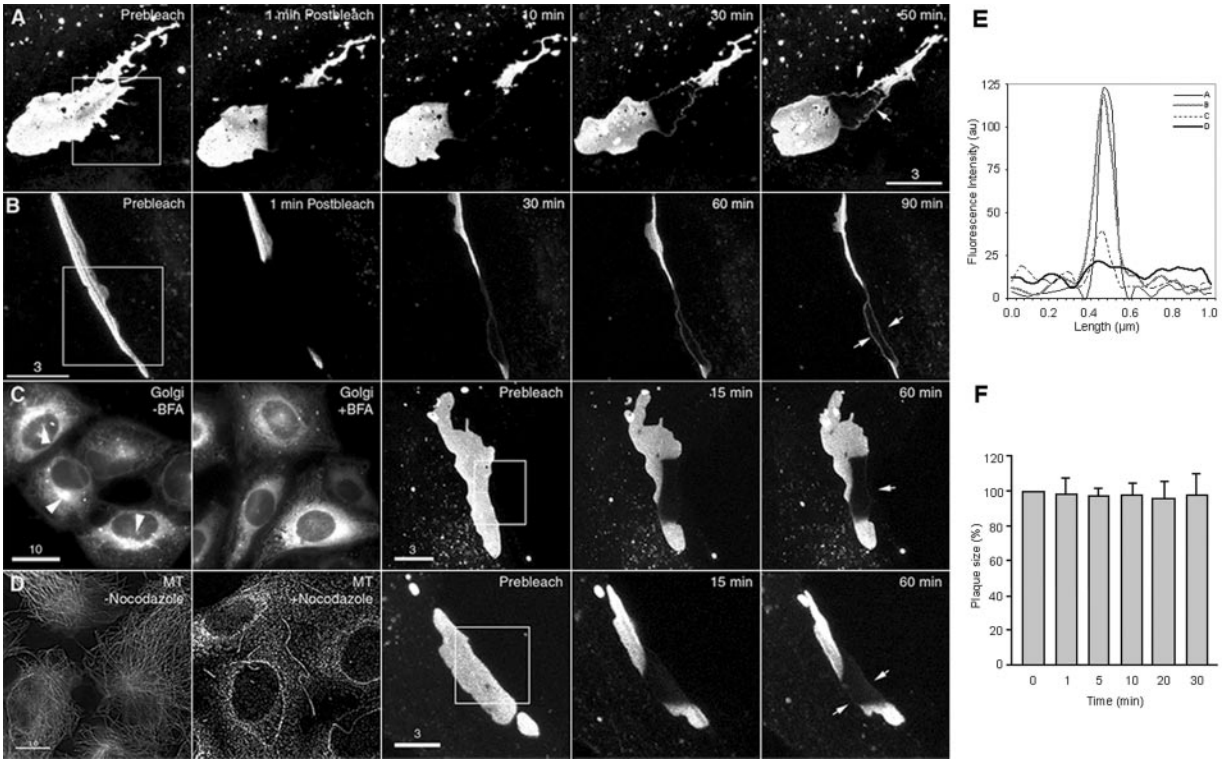

Fig. 2. Accrual of newly synthesized connexons to the outer margins of GJ channel clusters tracked in living cells. Fluorescence of selected areas (boxed) of GJs assembled from Cx43-GFP in transfected HeLa cells was permanently photo-bleached and recruitment of newly synthesized channels (denoted by arrows), shown in plane view in *A* and in edge view in *B*, was observed over time. Accrual of channels to the cluster in cells treated with BFA (*C*) or nocodazole (*D*). Disruption of the Golgi (labeled with arrowheads) and MTs was verified in treated cells before photo-bleaching (first two panels in *C* and *D*). (*E*) Amount of channels added to the plaque margins in *A–D* was determined by measuring total fluorescence intensity (in arbitrary units) along a line traversing one of the outer plaque margins in the last postbleach images. (*F*) The size of GJs was measured during the postbleach period by outlining bleached and recovered areas and unbleached plaques in the vicinity ($n = 6$) by polygons, and pixel-size of the polygons (in percent) was plotted over time. Bars in all figures are given in μm.

after a period of 10–20 min similar to that of untreated cells (Table 1); however, to a much lesser extent (≈20% of the recovery observed in untreated cells, Fig. 2*E*) resulting only in a thin, modestly fluorescent line along the bleached plaque areas that did not grow substantially wider and more fluorescent over time (Fig. 2*C*). Efficiency of plaque recovery in BFA-treated cells (nine plaques recover modestly, $n = 17$) was significantly reduced ($P = 0.028$, Fisher's exact test) compared with the recovery efficiency observed in untreated cells (19 plaques recover, 12 efficient, $n = 21$).

A comparable result was obtained when MTs were disrupted with nocodazole before photo-bleaching. MT disruption was verified by fluorescence microscopic observation (Fig. 2*D*, first two panels). Two of four plaques that were bleached recovered; however, recovery again remained modest. Fluorescence-recovery times were unaltered, and new edge-fluorescence was visible after a lag period of 15–20 min (Fig. 2 *D* and *E*, Table 1). Fluorescence recovery in Fig. 2 *A–D* was compared by measuring fluorescence intensities along a line traversing one of the plaque margins in the last postbleach images (Fig. 2*E*). Calculating the size of photo-bleached plaques and of plaques in their immediate vicinity over time indicated that plaques remained largely unaltered (Fig. 2*F*).

Table 1. Summary of photo-bleached gap junction plaques

No. of GJ plaques bleached	Pretreatment of cells*	Time plaques were observed after bleaching, min	No. of plaques stable 60 min after bleaching	No. of plaques bleached that remained stable†	No. of plaques in which accretion of channels was clearly visible after ≤30 min	Channel recruitment visible after, min	No. of GJ plaques in which channels moved by flow
32	None	10–120 (39 avg.)‡	28 (87.5%)	21	19 (90.4%) of 21 12 (63.2%) strong	5–30 (17 avg.)	18 of 25 (72.0%)
19	BFA	20–90 (45 avg.)	18 (94.7%)	17	9 (52.9%) of 17 None (0%) strong	10–30 (14 avg.)	5 of 17 (29.4%)
4	Nocodazole	30–60 (48 avg.)	4 (100%)	4	2 (50%) of 4 None (0%) strong	20 (20 avg.)	1 of 4 (25%)

*Cells were placed at least 30 min before photo-bleaching into medium containing the drug.
†Fluorescence in the scanned square area was bleached completely.
‡Average time period plaques were observed after photo-bleaching.

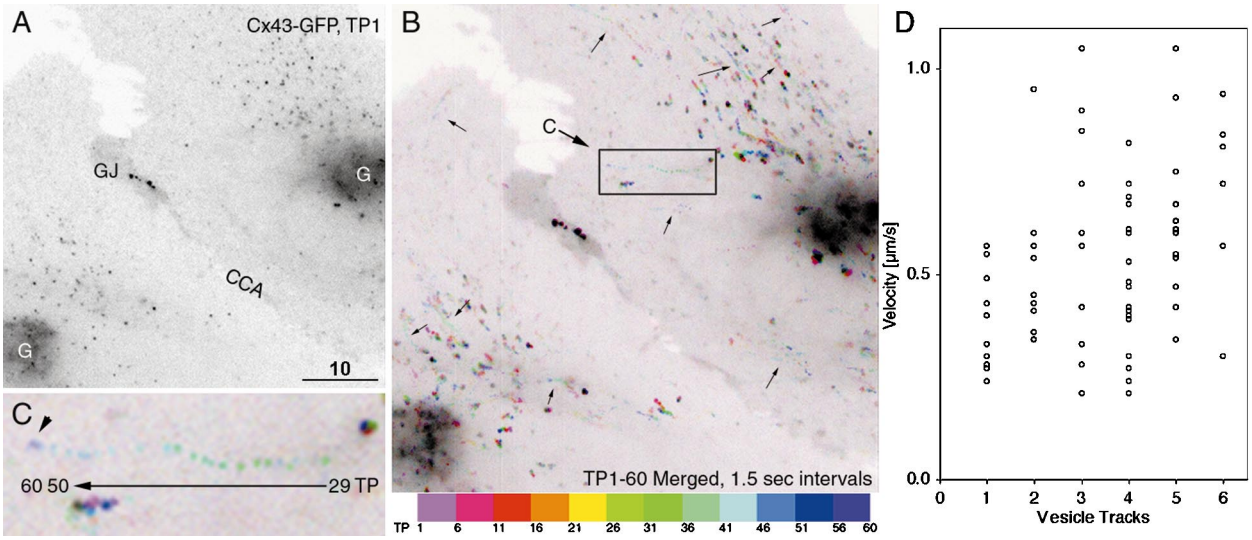

Fig. 3. Vesicular constitutive transport carriers deliver connexons from the Golgi to the PM. HeLa cells transfected with Cx43-GFP were imaged in the early phase of GJ assembly by rapid time-lapse microscopy. Many vesicular (*A*) and occasionally tubular transport containers (see Fig. 6, which is published as supporting information on the PNAS web site) exited the Golgi (G) and were transported in all directions, predominantly distant from GJs (GJ) and cell–cell appositions (CCA), into the periphery of the cells (see Movie 1). (*B*) Trails (depicted with arrows) and directional movement of secretory vesicles was visualized by color coding and merging the images of the time-lapse recording. (*C*) The track of a single vesicle traveling 11 μm in 31 s from time point (TP) 29–50. Preceding fusion, the vesicle becomes tethered (marked with an arrowhead) and only moves locally, restrained from TP 50–60. (*D*) Velocity plot of vesicle movement. The instantaneous speed of six vesicles moving saltatory along tracks was measured and plotted in distance traveled per second. Black and white was inverted in the images and Movie 1.

Connexons Traffic in Vesicular Structures Along MTs to Reach the PM. To investigate where the newly accrued GJ channels originated, we investigated secretory Cx43-GFP trafficking in living cells. HeLa cells actively assembling GJs were imaged early after transfection when a pool of Cx43-GFP connexons had accumulated in the Golgi region and small GJ plaques began to assemble at PM appositions. When cells were imaged at a frame rate of $\geq$1 image every 5 s, numerous Cx43-GFP containing vesicular structures were observed to exit the Golgi region and to traffic away from the Golgi into the periphery of the cells (Fig. 3*A* and Movie 1, which is published as supporting information on the PNAS web site). Golgi-exit occurred un-directional and most transport occurred in the cell body (Fig. 3*B*). In some of our recordings transport occurred along preferred transport routes that reached the PM distant from cell–cell appositions (see Fig. 6 and Movie 4, which are published as supporting information on the PNAS web site). Most of the post-Golgi cargo containers were round and had a diameter of no more than 200 nm (Fig. 3*A*). Occasionally, elongated cargo containers were observed to exit the Golgi (see *Supporting Text* and Fig. 6). Cx-containing transport containers traveled saltatory, predominantly directional along curvilinear tracks, indicative of trafficking along MTs (Fig. 3 *A* and *B*). Movements were fast, $\approx$0.5 μm/s in average (min = 0.2 μm/s, max = 1.05 μm/s, mean = 0.51 $\pm$ 0.22 μm/s) (Fig. 2*D*). Vesicle tracks, and direction of movement away from the Golgi were clearly visible when images covering a time period of about 90 s were color-coded and superimposed (Fig. 3 *B* and *C*).

That Cx-containing secretory vesicles indeed were traveling along MTs was demonstrated when their movement was imaged in living cells in which MTs were labeled with YFP-tubulin (Fig. 4*A*). While a number of larger vesicular structures, proposed to be degradation products (14), moved within the perinuclear region of the cell, several smaller vesicles trafficked toward the plus ends of MTs and into the periphery of the cell (Fig. 4*A*, and see Movie 2). The path of such a secretory vesicle is tracked in Fig. 4*A*. Based on a number of characteristics, degradative vesicular structures could be distinguished clearly from constitutive carriers (described in supporting materials). Wild-type

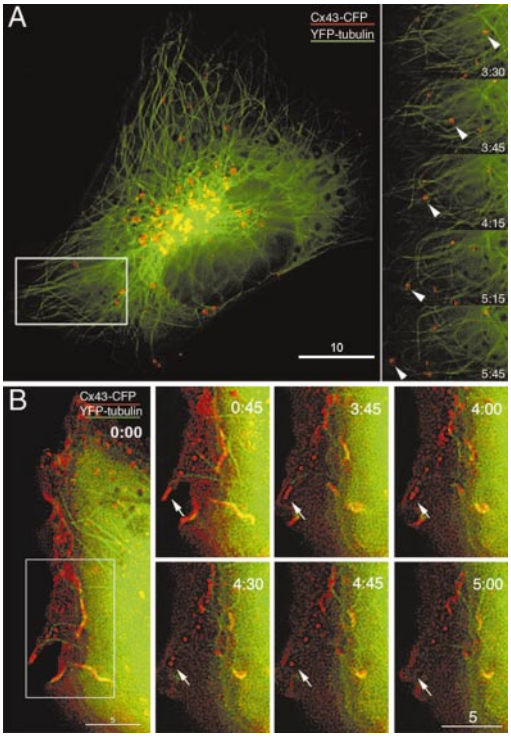

Fig. 4. Constitutive Cx43 containing transport carriers move along MTs and deliver connexons into the nonjunctional PM. (*A*) In HeLa cells transfected with Cx43-CFP (red) and YFP-tubulin (green), vesicular constitutive carriers and larger degradative structures associated closely with, and moved along MTs (see Movie 2, which is published as supporting information on the PNAS web site). Trails of Cx43-CFP vesicles moving overall away from the Golgi are evident. A slower migrating Cx43-GFP carrier (marked with arrowhead) traveling up to 0.58 μm/s away from the Golgi into the cell periphery is tracked. (*B*) Vesicular constitutive Cx43-CFP-containing carriers traveling along a MT that extends to the PM was imaged in 15-s intervals. Vesicles gathered at the end before, one after the other, fused with the nonjunctional PM (depicted with an arrow; see Movie 3, which is published as supporting information on the PNAS web site).

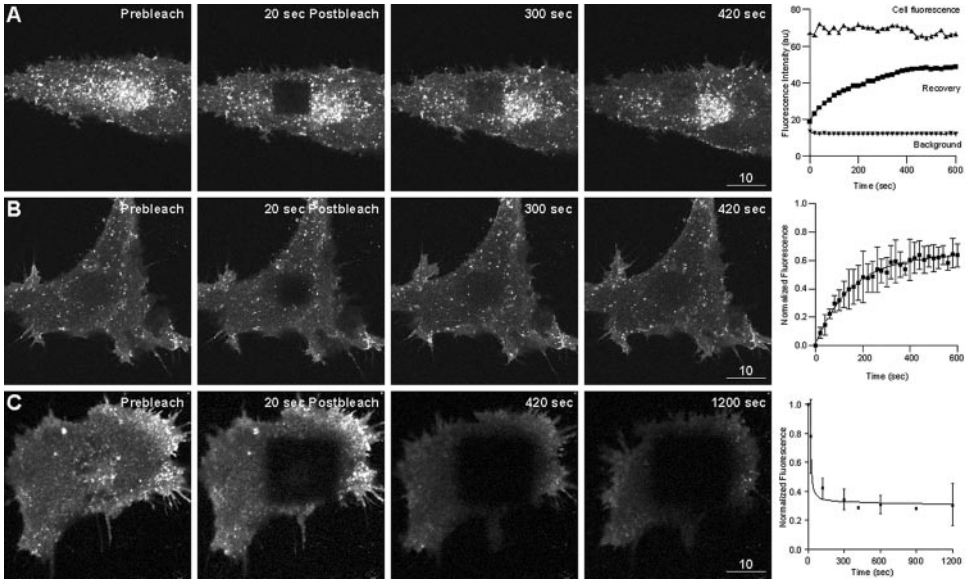

Fig. 5. Qualitative FRAP and FLIP experiments indicate that connexons delivered into the nonjunctional PM move freely. Confocal sections focused on the PM of HeLa cells expressing Cx43-GFP are shown. Besides a homogenous fluorescence indicative of dispersed connexons in the PM, larger bright fluorescent spots representing intracellular vesicular structures and possibly Cx43-GFP aggregates are visible. (*A*) After photo-bleaching of square areas, unbleached connexons diffuse into the bleached areas, whereas bright fluorescent spots remain largely immobile. (*B*) Mobile and immobile PM fluorescence fractions were calculated from cells in which intracellular fluorescence was prebleached. (*C*) Loss of PM fluorescence (FLIP) was calculated by photo-bleaching a selected square area repeatedly within 20 min, and fluorescence intensity of the cell outside the bleached area was measured over time. Experiments were quantified and fluorescence intensity (in arbitrary units in *A*) or normalized fluorescence intensities (as a ratio in *B* and *C*) were plotted over time.

Cx43, expressed endogenously in T51B liver epithelial cells also associated with MTs, suggesting that wild-type Cx43 is also delivered to the PM in vesicular carriers that traffic along MTs (see Fig. 7, which is published as supporting information on the PNAS web site).

Connexon-Containing Transport Carriers Fuse with Nonjunctional PMs. In time-lapse recordings of cells actively assembling GJs, Cx43-GFP-containing carriers appeared to tether to the PM after moving into the periphery of the cells. Tethering was indicated by a larger, irregularly shaped dot at the end of a vesicle track in superimposed time-lapse sequences (marked with an arrowhead in Fig. 3*C*) that is likely to originate from the locally restrained movement of the tethered vesicle (16, 17). Fluorescence of some of these vesicular carriers suddenly disappeared, suggesting membrane fusion (18). We also observed Cx43-CFP-containing constitutive transport containers to gather at the end of YFP-tubulin-labeled MTs that extended into the nonjunctional PM periphery, and one after the other to fuse with the PM. PM fusion again was indicated by their sudden disappearance (see Fig. 4*B*, Movie 3, and *Supporting Text*).

Connexons Delivered to the PM Can Move Freely. When HeLa cells expressing Cx43-GFP were focused on their membrane surface, homogenous fluorescence distributed over the entire PM was detected besides larger, brightly fluorescent spots that were often concentrated around the cell nucleus (Fig. 5 *A–C*). Confocal z-sectioning and mobility measurements (see below) indicated that the homogenous fluorescence is likely to originate from connexons that were delivered to, and randomly dispersed over the entire PMs of the cells (Fig. 5 *A–C*), whereas the bright spots are likely to represent intracellular vesicular structures (mainly degradative vesicular structures) close to the PM surface and possibly connexin aggregates that were dramatically reduced in number when the focal plane was placed higher, and more outside of the cells (compare Fig. 5 *A* with *B* and *C*). When fluorescence of PM square areas (9×9 μm) was permanently photo-bleached in living cells ($n = 15$), edges of the bleached areas faded rapidly, and PM fluorescence recovered equally from all sides within 6–7 min after bleaching (Fig. 5 *A* and *B*). Bright spots were largely immobile, or moved only slowly (Fig. 5*A*), indicating that they were not the units that were added to GJs. No recovery occurred in formaldehyde-fixed cells (data not shown). To better assess the amount of mobile and immobile fractions in the PM, total fluorescence within a square area was photo-bleached, and after recovery was bleached again before recovery was imaged. Under these conditions fluorescence within the square area recovered in average to ≈70% ($n = 3$; Fig. 4*B*), indicating that PM fluorescence was largely mobile. Similar results were obtained when PM square areas were bleached repeatedly over a period of 20 min and loss of fluorescence (FLIP) in unbleached areas of the cells ($n = 2$) was monitored (Fig. 5*C*).

Discussion

We used FRAP to investigate the addition of connexons to existing GJ channel clusters. We found that newly synthesized channels were accrued to the outer margins of channel clusters (as depicted in Fig. 1 *B* and *C*). Newly added channels were recognizable by their GFP fluorescence, forming fluorescent lines outlining the older, bleached cluster areas (Fig. 2). Fluorescence reappeared homogeneously throughout the entire length of the bleached areas as a solid, fine line that steadily increased in width (Fig. 2 *A* and *B*), indicating that connexons were added as single particles, or in very small groups consistent with the homogenous distribution of connexons in the plasma membrane (see below). Flow of channels from the unbleached areas along the outer margins into the bleached areas can be excluded (see supporting information). Reappearance of small fluorescent domains within the channel clusters, indicative of fusion of connexons containing secretory vesicles within the channel cluster (as depicted in Fig. 1*A*), was not observed.

The size of the photo-bleached plaques remained relatively constant over the postbleach observation period (Fig. 2*F*),

indicating that GJ plaques had reached a steady-state in which removal of older, photo-bleached channels in the center and accrual of newly synthesized channels to the cluster margins was in balance. This is in agreement with observations of Gaietta *et al.* (19) who also found that GJs were replenished from the outer margins and older channels were removed from the center without significant increase of cluster size over time. In our experiments, the recovered stripe of channels reached a width of up to 0.5 μm within 1 h, indicating that up to 50 layers of channels were added, if channels have a predicted center-to-center spacing of $\approx$10 nm (5). This means that a GJ 1 μm^2 in size that consists of $\approx$10,000 channels could be assembled within 2 h. This is somewhat faster than the replenishment observed by Gaietta *et al.* (19) who found that a 0.5–1.5-μm-wide border was added within 4 h. The difference in channel accrual in the two studies might be due to a higher protein synthesis rate that is suggested by the larger plaque size in our cells, or the limited resolution of light microscopy that might artificially increase the width of the fluorescent channel rim.

To investigate whether channel accrual depended on delivery of connexons to the PM, we inhibited secretion of newly synthesized connexons by disrupting MTs with nocodazole, or by treating the cells with BFA before photo-bleaching. BFA disrupts the Golgi apparatus by vesiculating the Golgi membranes that then rapidly redistribute into the endoplasmic reticulum (20, 21). Previously, it has been shown that Cxs pass through the Golgi, that Cx PM delivery is inhibited by BFA treatment, and that intracellular assembly of Cxs into connexons is a prerequisite for successful delivery to the PM (7–12). Also, under these conditions plaques initially recovered fluorescence along their margins within 10–20 min; however, further recovery was inhibited. This suggests that a pool of newly synthesized connexons is present in PMs that can accrue to the edge of plaques, and that further connexon accrual depends on the delivery of newly synthesized connexons when the PM connexon pool becomes depleted.

To further investigate whether connexons indeed were delivered to nonjunctional PMs as suggested by the recovery in BFA and nocodazole-treated cells (as depicted in Fig. 1*C*), or were trafficked directly to the outer rim of the channel clusters (as depicted in Fig. 1*B*), we investigated delivery of connexons to the PM by time-lapse microscopy. We found that connexons exit the Golgi region predominantly in vesicular carriers that traffic along MTs to reach the PM. Post-Golgi trafficking along MTs and similar constitutive carrier characteristics were described recently for nonoligomeric membrane proteins traversing the PM bilayer once (refs. 18 and 22; also see supporting information).

PM insertion of connexons appeared to occur predominantly distributed over the entire nonjunctional PM surface, consistent with the delivery of a number of membrane proteins including aquaporin-1 (23), vesicular stomatitis virus G (VSVG) protein (16–18), and glycosyl phosphatidyl inositol (GPI)-anchored proteins (22). FRAP and FLIP experiments indicated that PM connexons can move laterally in the plane of the membrane, consistent with the movement of diffusing proteins in cellular membranes (24–27), and thus, can reach the outer margins of GJ channel clusters. The fast FRAP and FLIP kinetics, as well as the homogeneity of the recovered fluorescence, indicate that connexons are distributed as single particles, or small groups, but not as large aggregates. This finding was also indicated by the mode of fluorescence recovery along the channel cluster margins described above.

Delivery of connexons into the PM instead of routing them directly to GJs might be unexpected, especially because MTs can anchor directly at Cx43-based GJs (28). However, connexons were not observed to exit the Golgi into any specific direction, and many more MTs reach the PM periphery without attaching to GJ plaques (28). Furthermore, a number of recent reports describe the presence of connexons in the PM that function there as independent entities to regulate intra- and extracellular milieus (29–31). Thus, delivery of connexons to the nonjunctional PM provides a simple two-step mechanism that allows connexons to function in intra-/extracellular signaling, as well as in direct cell–cell communication. In many electron microscopic images of GJ freeze–fracture replicas that were obtained from tissues, intermembranous particles can be seen dispersed around GJ channel clusters that can be interpreted as individual GJ channels or connexons (see, e.g., refs. 32 and 33), and may reflect the pool of dispersed connexons in the PM and the accretion of channels to the plaque that we have observed in living cells.

This work was supported by grants from the National Institutes of Health (to M.M.F. and S.-C.C.) and an International Union Against Cancer travel fellowship (to B.N.G.G.).

1. Goodenough, D. A. & Revel, J. P. (1970) *J. Cell Biol.* **45,** 272–290.
2. McNutt, N. S. & Weinstein, R. S. (1970) *J. Cell Biol.* **47,** 666–688.
3. Friend, D. S. & Gilula, N. B. (1972) *J. Cell Biol.* **53,** 758–776.
4. Gilula, N. B., Reeves, O. R. & Steinbach, A. (1972) *Nature (London)* **235,** 262–265.
5. Unger, V. M., Kumar, N. M., Gilula, N. B. & Yeager, M. (1999) *Science* **283,** 1176–1180.
6. Willecke, K., Eiberger, J., Degen. J., Eckardt, D., Romualdi, A., Guldenagel, M., Deutsch, U. & Sohl, G. (2002) *Biol. Chem.* **383,** 725–737.
7. Falk, M. M., Kumar, N. M. & Gilula, N. B. (1994) *J. Cell Biol.* **127,** 343–355.
8. Musil, L. S. & Goodenough, D. A. (1993) *Cell* **74,** 1065–1077.
9. Falk, M. M., Buehler, L. K., Kumar, N. M. & Gilula, N. B. (1997) *EMBO J.* **16,** 2703–2716.
10. Musil, L. S. & Goodenough, D. A. (1991) *J. Cell Biol.* **115,** 1357–1374.
11. Laird, D. W., Castillo, M. & Kasprzak, L. (1995) *J. Cell Biol.* **131,** 1193–1203.
12. Falk, M. M. (2000) *J. Cell Sci.* **113,** 4109–4120.
13. Falk, M. M. (2000) *Eur. J. Cell Biol.* **79,** 564–574.
14. Jordan, K., Solan, J. L., Dominguez, M., Sia, M., Hand, A., Lampe, P. D. & Laird, D. W. (1999) *Mol. Biol. Cell* **10,** 2033–2050.
15. Bukauskas, F. F., Jordan, K., Bukauskiene, A., Bennett, M. V., Lampe, P. D., Laird, D. W. & Verselis, V. K. (2000) *Proc. Natl. Acad. Sci. USA* **97,** 2556–2561.
16. Schmoranzer, J., Goulian, M., Axelrod, D. & Simon, S. M. (2000) *J. Cell Biol.* **149,** 23–32.
17. Toomre, D., Steyer, J. A., Keller, P., Almers, W. & Simons, K. (2000) *J. Cell Biol.* **149,** 33–40.
18. Toomre, D., Keller, P., White, J., Olivo, J. C. & Simons, K. (1999) *J. Cell Sci.* **112,** 21–33.
19. Gaietta, G., Deerinck, T. J., Adams, S. R., Bouwer, J., Tour, O., Laird, D. W., Sosinsky, G. E., Tsien, R. Y. & Ellisman, M. H. (2002) *Science* **296,** 503–507.
20. Lippincott-Schwartz, J., Yuan, L. C., Bonifacino, J. S. & Klausner, R. D. (1989) *Cell* **56,** 801–813.
21. Sciaky, N., Presley, J., Smith, C., Zaal, K. J., Cole, N., Moreira, J. E., Terasaki, M., Siggia, E. & Lippincott-Schwartz, J. (1997) *J. Cell Biol.* **139,** 1137–1155.
22. Keller, P., Toomre, D., Diaz, E., White, J. & Simons, K. (2001) *Nat. Cell Biol.* **3,** 140–149.
23. Deen, P. M., Nielsen, S., Bindels, R. J. & van Os, C. H. (1997) *Pflugers Arch.* **433,** 780–787.
24. Zhang, F., Crise, B., Su, B., Hou, Y., Rose, J. K., Bothwell, A. & Jacobson, K. (1991) *J. Cell Biol.* **115,** 75–84.
25. Storrie, B., Pepperkok, R., Stelzer, E. H. & Kreis, T. E. (1994) *J. Cell Sci.* **107,** 1309–1319.
26. Cole, N. B., Smith, C. L., Sciaky, N., Terasaki, M., Edidin, M. & Lippincott-Schwartz, J. (1996) *Science* **273,** 797–801.
27. Ellenberg, J., Siggia, E. D., Moreira, J. E., Smith, C. L., Presley, J. F., Worman, H. J. & Lippincott-Schwartz, J. (1997) *J. Cell Biol.* **138,** 1193–1206.
28. Giepmans, B. N., Verlaan, I., Hengeveld, T., Janssen, H., Calafat, J., Falk, M. M. & Moolenaar, W. H. (2001) *Curr. Biol.* **11,** 1364–1368.
29. Quist, A. P., Rhee, S. K., Lin, H. & Lal, R. (2000) *J. Cell Biol.* **148,** 1063–1074.
30. Kamermans, M., Fahrenfort, I., Schultz, K., Janssen-Bienhold, U., Sjoerdsma, T. & Weiler, R. (2001) *Science* **292,** 1178–1180.
31. Contreras, J. E., Sanchez, H. A., Eugenin, E. A., Speidel, D., Theis, M., Willecke, K., Bukauskas, F. F., Bennett, M. V. & Saez, J. C. (2002) *Proc. Natl. Acad. Sci. USA* **99,** 495–500.
32. Hulser, D. F., Rehkopf, B. & Traub, O. (1997) *Exp. Cell Res.* **233,** 240–251.
33. Benedetti, E. L., Dunia, I., Recouvreur, M., Nicolas, P., Kumar, N. M. & Bloemendal, H. (2000) *Eur. J. Cell Biol.* **79,** 575–582.

Supporting Text

Materials and Methods

Cell Lines. A stable HeLa-22 cell line generated in the Tet-On gene expression system (CLONTECH) in which the expression of Cx43-GFP could be regulated has been used in this study as well. Cx43-GFP behaved similar in stable and transiently expressing cells, both with respect to Golgi accumulation and trafficking, as well as plaque recovery after photo-bleaching. However, transiently transfected cells were overall noticeably brighter, and thus were used in most studies.

Results and Discussion

Recovery of Fluorescence Along the Outer Margins of GJ Channel Clusters. Flow of channels from the unbleached areas along the outer margins into the bleached areas would have resulted in an initially stronger fluorescence reappearance in the vicinity of the unbleached areas, and not in a homogenous recovery along the entire bleached area and can be excluded.

Characteristics of Degradative Cx43-GFP Containing Vesicular Structures. Degradative vesicular structures could clearly be distinguished from constitutive carriers in our time-lapse experiments because they were larger, approximately 0.25–1 μ m in diameter, often irregularly shaped, and their fluorescence was brighter. Although these vesicular structures also traveled along MTs, they moved much slower than the constitutive carriers with an average speed of only ≈ 0.1 μ m/s, and much less directional (Fig. 4*A* and Movie 2). Many of these vesicular bodies colocalized with acidic subcellular structures (stained with Lysotracker), supporting the conclusion that they were degradative structures, such as endosomes and lysosomes (data not shown).

Constitutive Vesicle Fusion with the Plasma Membrane. Although we have not observed the actual fusion event of constitutive connexon-containing vesicles with the PM, membrane fusion was indicated. Retrograde transport of Cx43-CFP-containing cargo vesicles along MTs back into the cell body would have been visible on the image sequences shown in Fig. 4*B* and can clearly be excluded. Movement of the vesicles out of the focal plane can also be excluded because the entire thickness of the cell periphery is covered in a single image. Constitutive cargo vesicle fusion with the PM was recently imaged using Total Internal Reflection Fluorescence (TIRF) microscopy (1–3). The fusion of VSVG-GFP-containing cargo vesicles with the PM was observed to be short, lasting <1 s and resulted in a local rise of fluorescence intensity that rapidly diffused into the PM (1, 2). Because of this short event, it would have been very difficult to observe the actual fusion process in recordings such as the one shown in Fig. 4*B* that was acquired with 15 s intervals. Furthermore, Cxs are delivered as hexameric structures that may reduce the rise in fluorescence intensity that has been seen upon VSVG protein fusion. Finally, we do not know how many connexons are packed into a typical cargo vesicle, and whether connexons, once inserted into the PM, diffuse as rapidly as VSVG protein.

References

1. Schmoranzer, J., Goulian, M., Axelrod, D. & Simon, S. M. (2000) *J. Cell Biol.* **149,** 23–32.
2. Toomre, D., Steyer, J. A., Keller, P., Almers, W. & Simons, K. (2000) *J. Cell Biol.* **149,** 33–40.
3. Keller, P., Toomre, D., Diaz, E., White, J. & Simons, K. (2001) *Nat. Cell Biol.* **3,** 140–149.
4. Toomre, D., Keller, P., White, J., Olivo, J. C. & Simons, K. (1999) *J. Cell Sci.* **112,** 21–33.
5. Sciaky, N., Presley, J., Smith, C., Zaal, K. J., Cole, N., Moreira, J. E., Terasaki, M., Siggia, E. & Lippincott-Schwartz, J. (1997) *J. Cell Biol.* **139,** 1137–1155.
6. Falk, M. M. (2000) *J. Cell Sci.* **113,** 4109–4120.

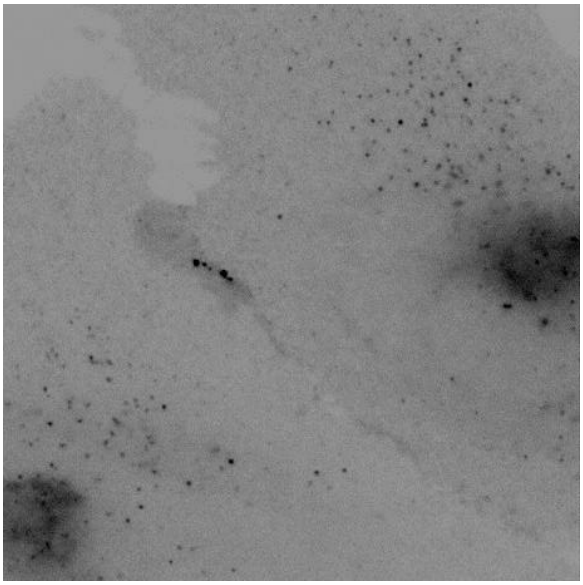

Movie 1 (accompanying Fig. 3). Vesicular constitutive transport carriers deliver connexons from the Golgi to the plasma membrane. HeLa cells transfected with Cx43-GFP were imaged in the early phase of gap junction assembly by rapid time-lapse microscopy. Two cells with small gap junction plaques assembled in the adjoining membranes (center) were imaged at steady state without pretreating cells with drugs. Many vesicular transport containers exited the Golgi (dark areas at top right and bottom left) and were transported in all directions, predominantly distant from gap junctions and cell–cell appositions (center) into the periphery of the cells. The movie covers 90 s of the time-lapse recording. Frames were acquired every 1.5 s. Frame width, 50 μm. Black and white was inverted for clarity in the movie sequence.

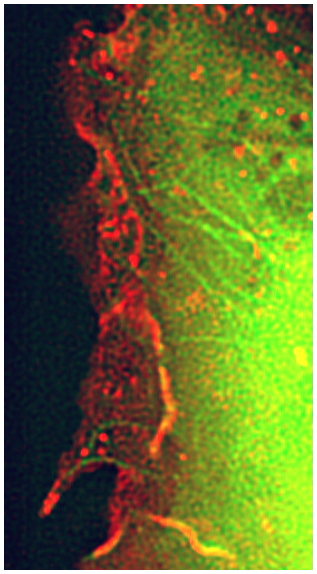

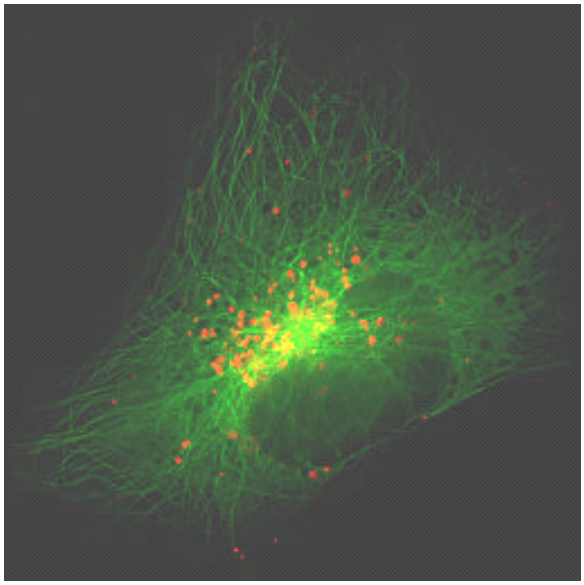

Movie 2 (accompanying Fig. 4*A*). Constitutive Cx43 containing transport carriers move along microtubules and deliver connexons into the nonjunctional plasma membrane. In HeLa cells transfected with Cx43-CFP (red) and YFP-tubulin (green), vesicular constitutive carriers and larger degradative structures associated closely with, and moved along microtubules. A single HeLa cell is shown. Cx43-CFP-containing vesicles (red) moving overall away from the Golgi (dense area of microtubules in the center next to the nucleus appearing dark in the bottom half of the images) into the cell periphery are evident. The movie covers 10 min of the time-lapse recording. Frames were acquired every 15 s. Frame width, 50 μm.

Movie 3 (accompanying Fig. 4*B*). Constitutive Cx43 containing transport carriers deliver connexons into the nonjunctional plasma membrane. The outer periphery of a HeLa cell expressing Cx43-CFP (red) is shown. Vesicular constitutive Cx43-CFP-containing carriers (red vesicles) traveling along a microtubule (green) that reaches out into the plasma membrane periphery (lower left) were imaged. Vesicles gathered at the end, before one after the other suddenly disappeared, indicating their fusion with the plasma membrane. Fusion events were reported to be very short (<1 s) and were not captured in this movie sequence. The movie covers 7 min and 30 s of the time-lapse recording. Frames were acquired every 15 s. Frame width, 13 μm.

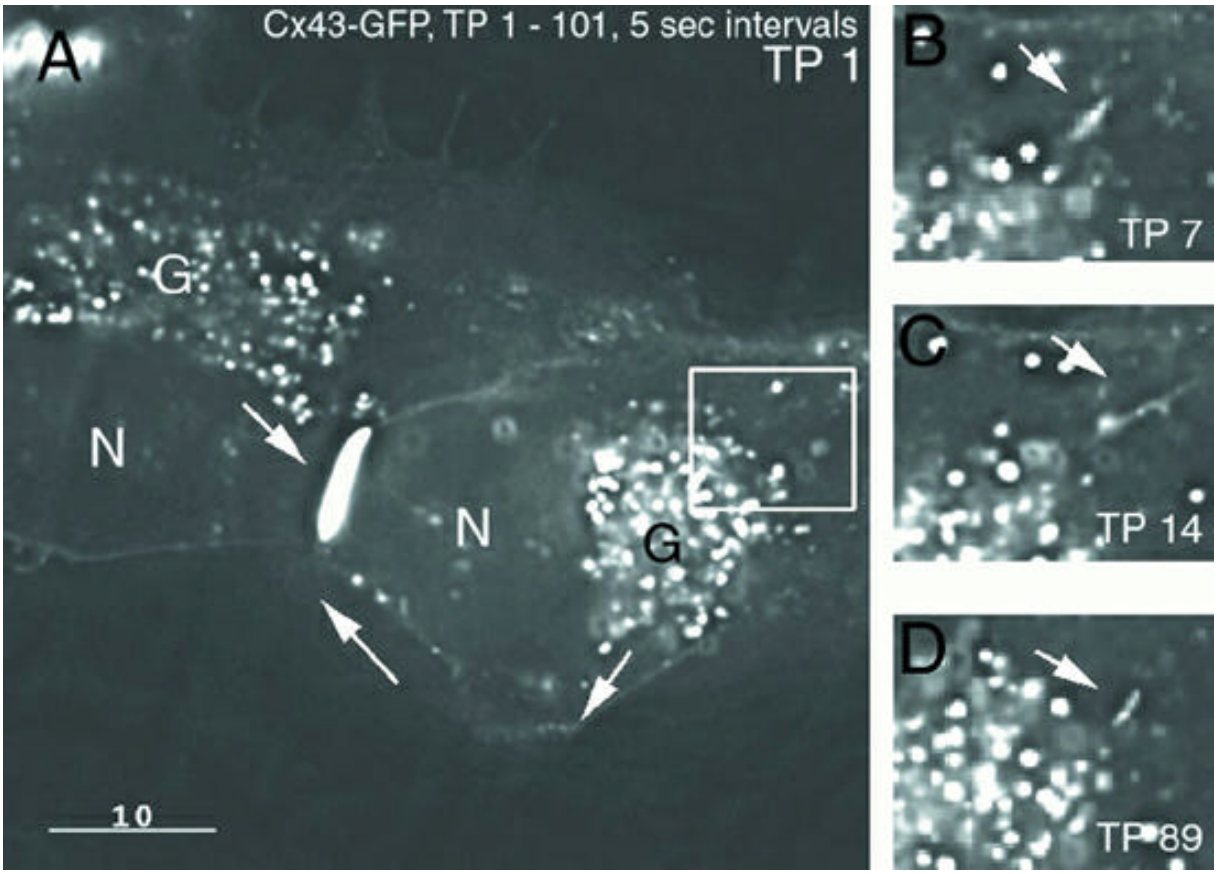

Movie 4 (accompanying Fig. 6). Connexin containing constitutive carriers traveling along p referred routs from the Golgi to the plasma membrane, then circumferential to reach gap junctions. Two HeLa cells expressing Cx43-GFP with a large gap junction plaque assembled in their adjoining plasma membranes (center) were imaged. Occasionally, tubular transport containers exited the Golgi region (see especially Golgi area at the right site of the frames), in addition to more common vesicular carriers, and trafficked into the periphery of the cells. In comparable studies that in addition describe a large number of tubular structures exiting the Golgi region, secretion was inhibited by keeping the cells at nonpermissive temperatures, or by treating the cells with BFA, whereas in this movie constitutive secretory Cx43-GFP trafficking under steady-state conditions was recorded. The movie covers 8 min and 25 s of the time-lapse recording. Frames were acquired every 5 s. Frame width, 52 μm.

Fig. 6. Cx43-GFP-containing carriers traveling along preferred routs from the Golgi (G) to the PM, then circumferential to reach GJs (depicted by arrows in *A*). In general, vesicular and only occasionally tubular transport containers (marked with arrows in *B*–*D*) exited the Golgi and trafficked into the periphery of the cell (Movie 4). In comparable studies that in addition describe a large number of tubular structures exiting the Golgi region, secretion was inhibited by keeping the cells at nonpermissive temperatures, or by treating the cells with BFA (3–5), while we have observed constitutive secretory Cx43-GFP traffic under steady-state conditions. BFA pretreatment has been reported to increase the number and size of secretory tubules extending from the Golgi (5).

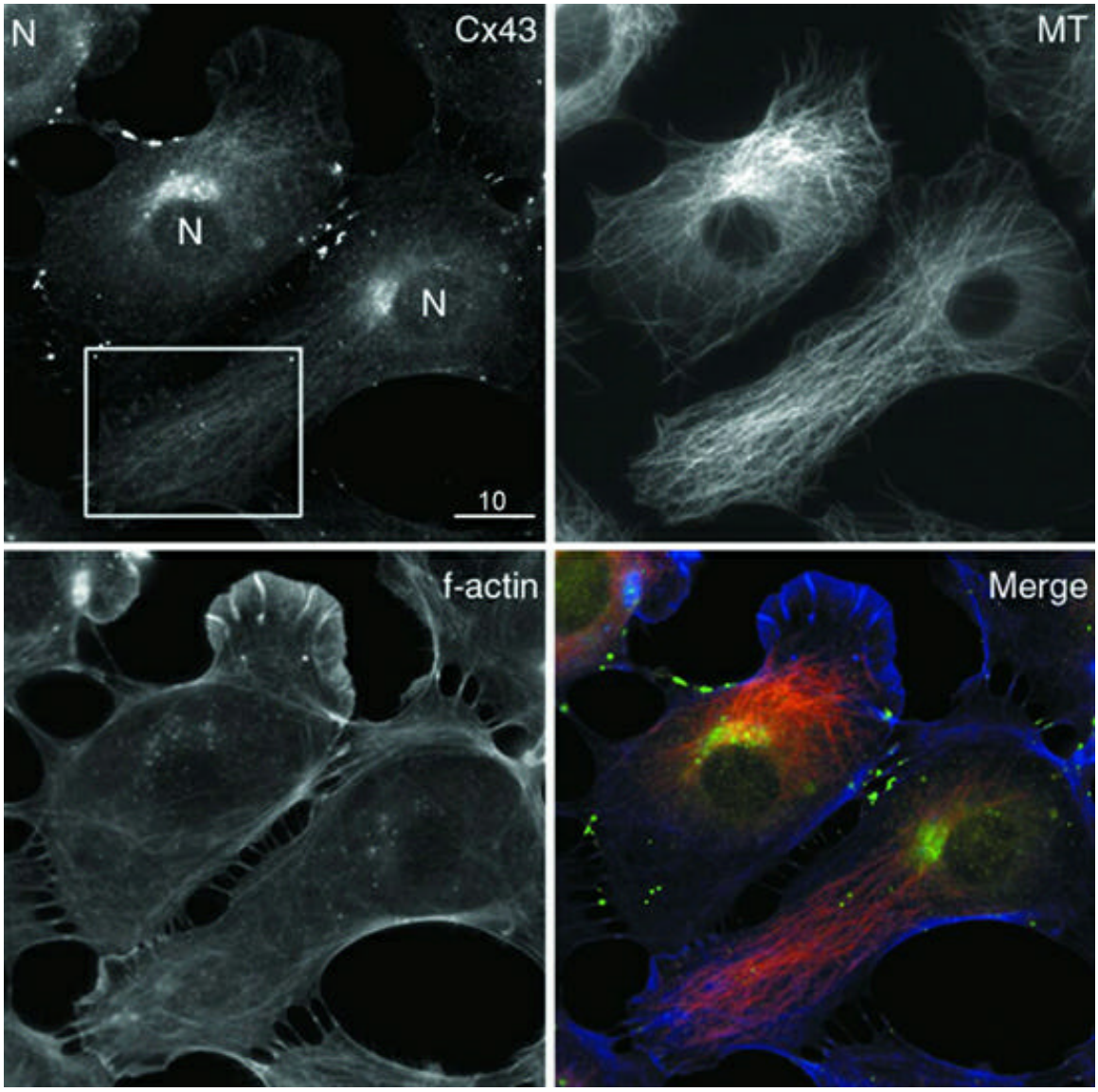

Fig. 7. Substantial amounts of intracellular Cx43 localize to MTs in cells that express endogenous Cx43 and actively assemble GJs. T51B cells were cultured for 24 h and processed for indirect immunofluorescence staining by using anti-Cx43 (green) and anti- -tubulin (red) antibodies and phalloidin to decorate F-actin (blue) as described below. A substantial amount of Cx43, most likely representing connexons in transit from the Golgi to the PM, localized to the Golgi (G) (located proximal to the nucleus [N] and appearing yellow in the merged image), and to MTs distributed throughout the cytoplasm of the cells (e.g. boxed area), but not to the actin cytoskeleton. Assembled GJs and GJ degradation products that are much larger than the secretory vesicles are visible as round and irregularly shaped green structures at appositional membranes and in the cytoplasm of the merged image. Cells were grown on cover glasses and processed as described (6). MTs were stained with monoclonal E7 antiserum (Developmental Studies Hybridoma Bank, University of Iowa, Iowa City) diluted 1:2 in PBS, and Cx43 was stained with a polyclonal antiserum (Zymed) diluted 1:200. AlexaFluor 647 (microtubules) and FITC (Cx43)-coupled secondary antibodies (Jackson Laboratories) were used in 1:100 to 1:200 dilutions. F-actin was decorated with a 1:200 dilution of rhodamine-phalloidin prepared in methanol (Molecular Probes).